Electronic Supplementary Information

Band Engineering of Mesoporous TiO_2 with Turnable Defects for Visible-Light Hydrogen Generation

Jin Yan[a], Lei Dai[a], Penghui Shi[a,b,*], Jinchen Fan[a], Yulin Min[a,b], Qunjie Xu[a,b,*]

[a] Shanghai Key Laboratory of Materials Protection and Advanced Materials in Electric Power, Shanghai University of Electric Power, Shanghai200090, P.R. China

[b] Shanghai Institute of Pollution Control and Ecological Security, Shanghai 200090, P.R. China

*Correspondence E–mail: shipenghui@shiep.edu.cn (P. Shi), xuqunjie@shiep.edu.cn (Q. Xu)

Table S1 below shows the particle size and unit cell parameters of Rh/B-TiO_2 with different doping amounts. XRD analysis demonstrates that all samples heated at 400 ℃ are in pure anatase phase and there is No observable structural difference between undoped and doped samples. The particle size obtained from the XRD data are assumed to be tetragonal crystal systems, which are listed in Table S1. The lattice expansion and contraction properties shown are consistent with previously reported B-doped TiO_2 data.

Table S1. Crystallite size and BET surface area of samples.

Products	Crystallite size (nm)	S_{BET} (m^2 g^{-1})
Pure TiO_2	46	43.14
B-TiO_2	51	139.05
Rh-TiO_2	39.3	82.55
$Rh_{0.1}$/B-TiO_2	28.7	195.01
$Rh_{0.5}$/B-TiO_2	25.9	381.55
Rh_1/B-TiO_2	17.6	198.54

Table S2. Parameters obtained from time-resolved PL decay curves according to a Three-exponential decay.

Sample	τ_1(ns)	τ_2(ns)	τ_3(ns)	A_1(%)	A_2(%)	A_3(%)	avlifetime(ns)
Pure TiO_2	186.16	926.98	35.38	67.51	94.76	99.54	346.43
B-TiO_2	128.56	840.26	18.75	66.28	94.46	99.50	299.19
B/$Rh_{0.5}$-TiO_2	196.73	1020.73	34.99	67.79	95.49	99.61	380.97

Transient PL B-TiO_2 and $Rh_{0.5}$/B-TiO_2 nanoporous particle decay curves are compared in Fig. 4c. And use the three exponential function to mathematically fit the PL decay curve:

$$y = A_1\exp(-x/\tau_1) + A_2\exp(-x/\tau_2) + A_3\exp(-x/\tau_3) + y_0 \qquad (1)$$

here A1, A2, A3 are amplitude coefficient and y_0 is basal constant. τ_1, τ_2 and τ_3 are the corresponding fluorescence lifetime, respectively. The calculated carrier lifetimes are shown in Table 2.After integrating through the formula, the average fluorescence lifetime is longer than other lifetimes:

$$\tau = \frac{A_1\tau_1^2 + A_2\tau_2^2 + A_3\tau_3^2}{A_1\tau_1 + A_2\tau_2 + A_3\tau_3} \qquad (2)$$

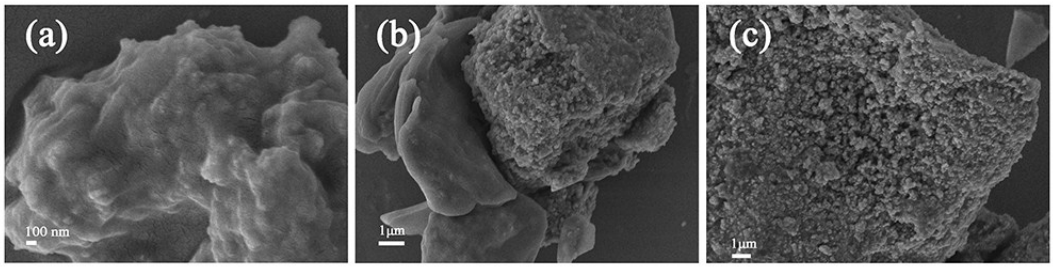

Fig. S1. The FESEM of pure TiO_2 (a) before annealing, (b) calcined for 1h, (c) after full annealing.

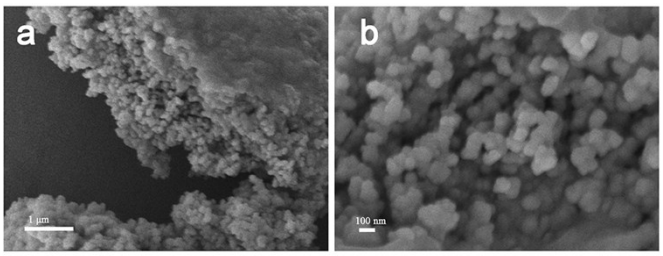

Fig. S2. The FESEM (a-b) images of the B doped-TiO_2 nanoparticle.

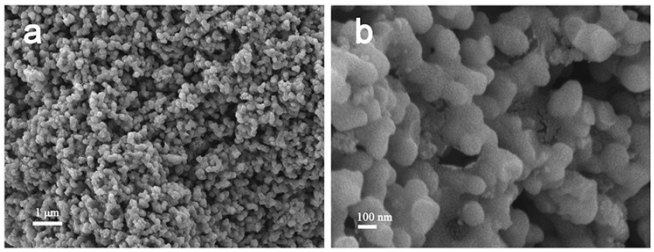

Fig. S3. The FESEM (a-b) images of the Rh-TiO_2 nanoparticle.

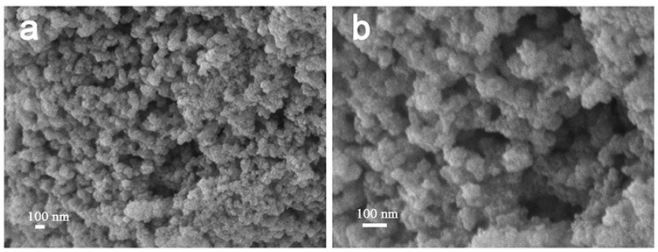

Fig. S4. The FESEM (a-b) images of the $Rh_{0.5}$/B codoped-TiO_2 nanoparticle.

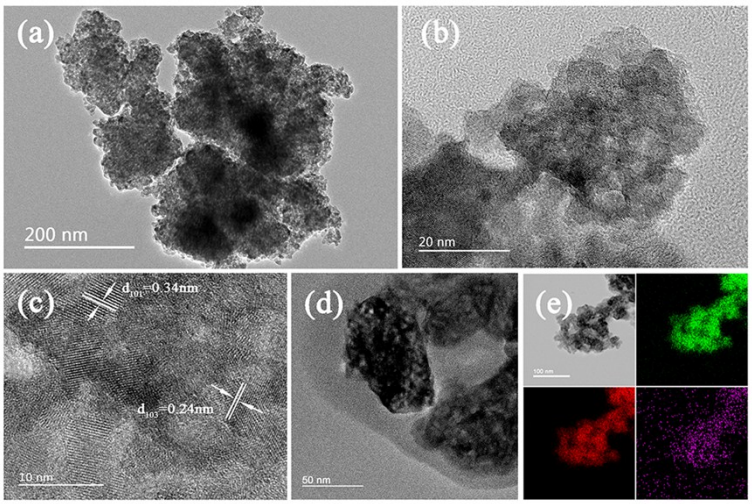

Fig. S5. The TEM image of B-TiO_2: (a, b,d) TEM; (c) HRTEM; (e) Mapping of B-doped TiO_2.

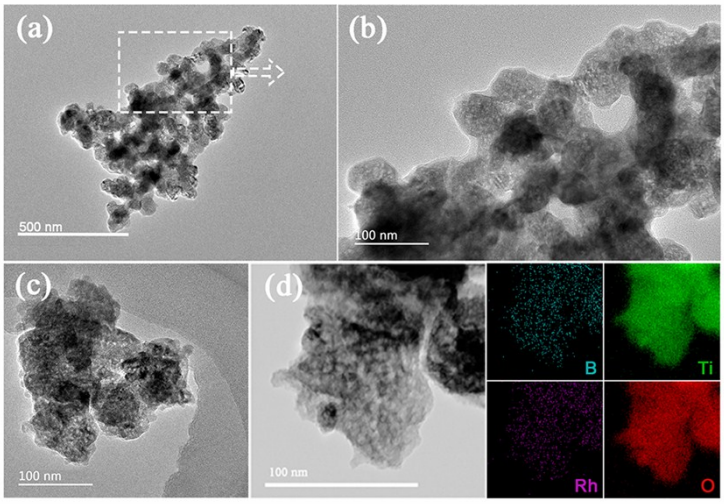

Fig. S6. The TEM of (a-b) B-TiO_2. (c) TEM, (d) mapping of Rh, B-codoped TiO_2.

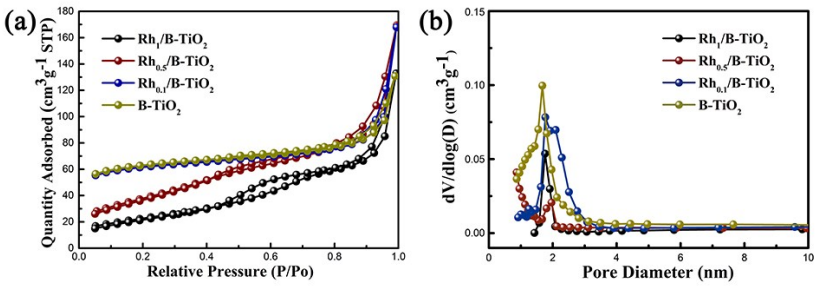

Fig. S7. (a) Nitrogen adsorption-desorption isotherms and (b) the corresponding pore size distribution curves of the Rhx/B-TiO2 (x=0, 0.1, 0.5, 1).

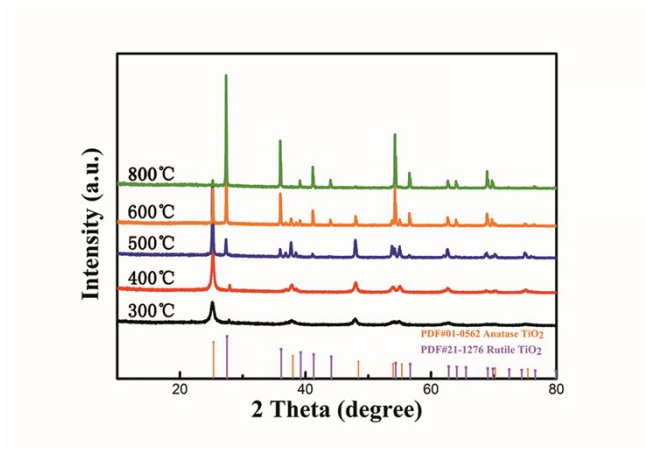

Fig. S8. XRD patterns of the TiO_2 at different temperatures.

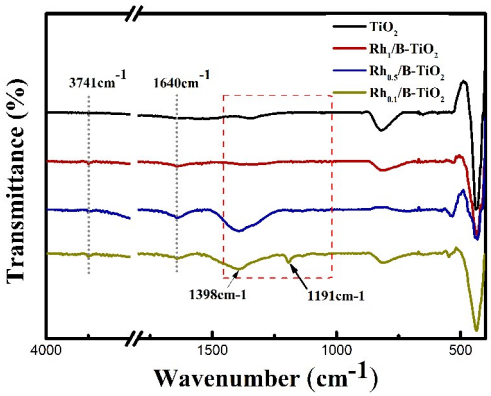

Fig. S9. FT-IR spectra of Rhx/B-TiO2 (x=0, 0.1, 0.5, 1).

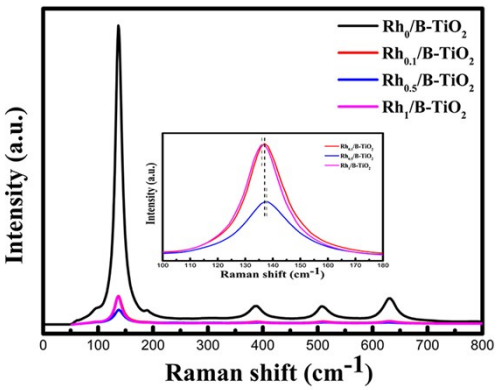

Fig. S10. Raman spectra of the Rh_x/B-TiO_2 (x=0, 0.1, 0.5, 1).

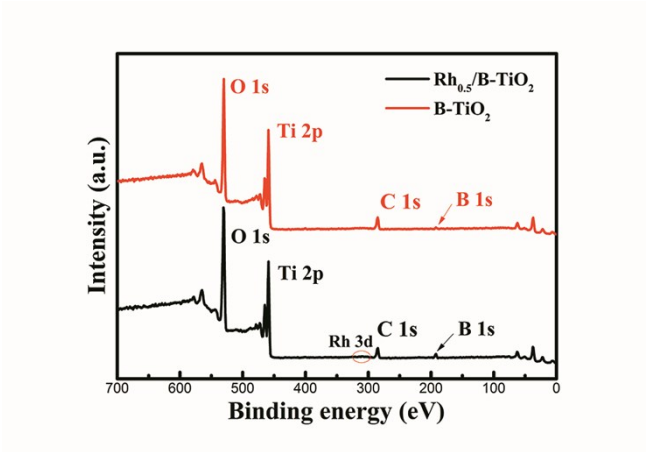

Fig. S11. XPS survey spectra of the B-TiO_2 and $Rh_{0.5}$/B-TiO_2.

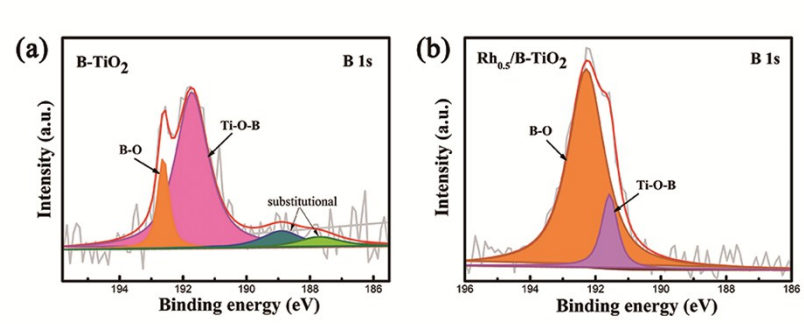

Fig. S12. High-resolution XPS spectra of B 1s for B-TiO_2 and $Rh_{0.5}$/B-TiO_2.

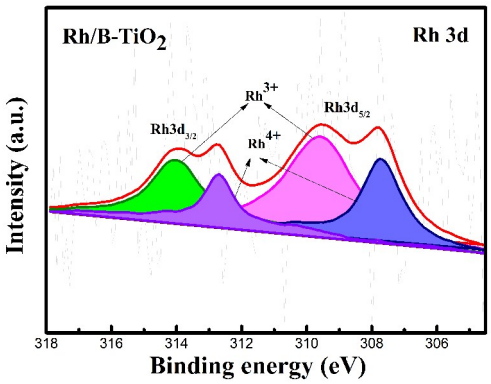

Fig. S13. High-resolution XPS spectra of Rh 3d for $Rh_{0.5}$/B-TiO_2.

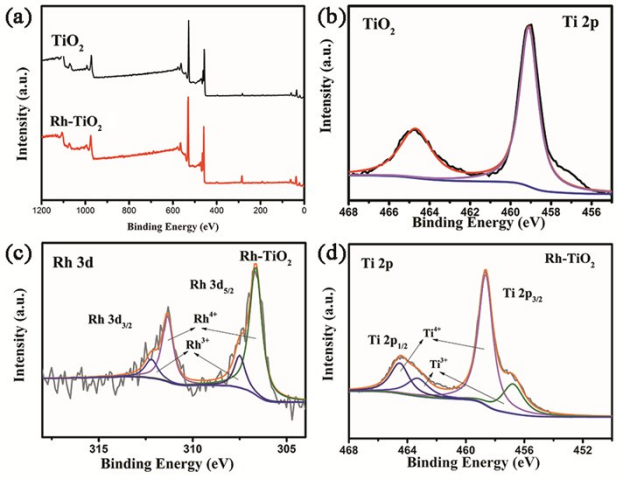

Fig. S14. High-resolution XPS spectra of pure TiO_2 and Rh-TiO_2.

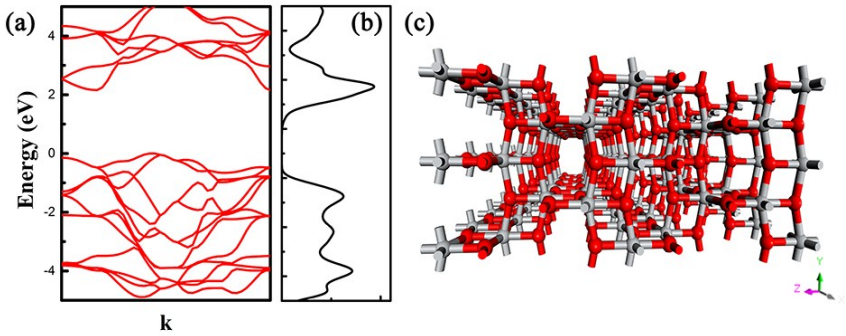

Fig. 15. (a-b) The energy band structure, DOS and (c) crystal structures of the pure TiO_2.

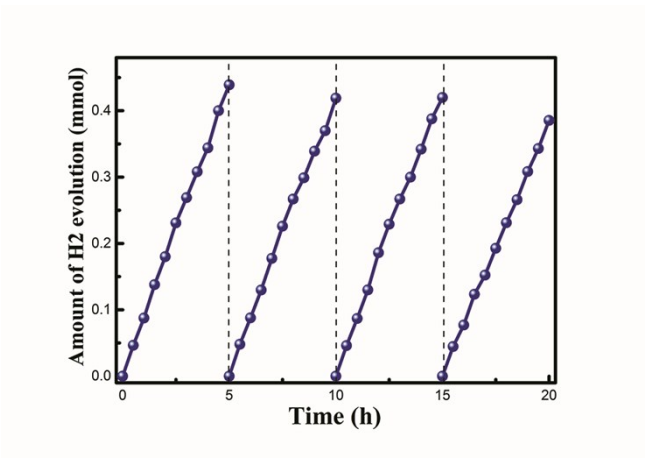

Fig. S16. Cycling tests of photocatalytic hydrogen evolution of $Rh_{0.5}$/B-TiO_2.

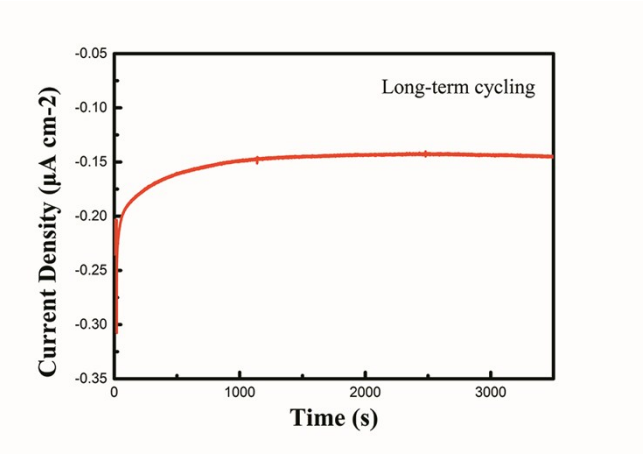

Fig. S17. Long-term cycling of transient photocurrents measurements of $Rh_{0.5}$/B-TiO_2.

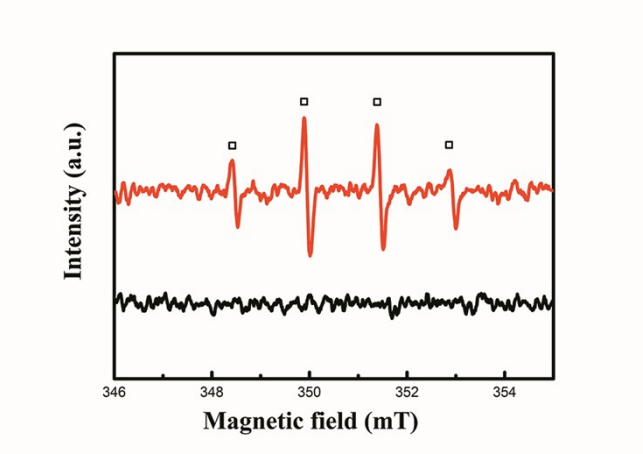

Fig. S18. EPR spectra with $Rh_{0.5}$/B-TiO_2.